ORGANOMETALLICS

pubs.acs.org/Organometallics Article

Steps Ahead in Understanding the Catalytic Isomerization Mechanism of Linear Allylic Alcohols in Water: Dynamics, Bonding Analysis, and Crystal Structure of an η^2-Allyl-Intermediate

Franco Scalambra, Belen Lopez-Sanchez, Nicole Holzmann, Leonardo Bernasconi, and Antonio Romerosa*

Cite This: *Organometallics* 2020, 39, 4491−4499 Read Online

ACCESS | Metrics & More | Article Recommendations | Supporting Information

ABSTRACT: The isomerization of 1-penten-3-ol into 3-pentanone catalyzed by $[RuCp(H_2O\text{-}\kappa O)(PTA)_2](CF_3SO_3)$ (**1CF$_3$SO$_3$**) (PTA = 1,3,5-triaza-7-phosphaadamantane) was studied and two water-soluble ruthenium catalyst reaction intermediates were characterized. The main intermediate, the complex $[RuCp(exo\text{-}\eta^2\text{-}1\text{-penten-3-ol})(PTA)_2](CF_3SO_3)\cdot 2H_2O$ (***exo*-2CF$_3$SO$_3$·2H$_2$O**), was isolated and characterized by NMR in solution and by single-crystal X-ray diffraction in the solid state, constituting the first example of a fully characterized complex containing a coordinated η^2-allylic alcohol and the first crystal structure for a water-soluble metal complex containing a η^2-allyl ligand. NMR and Eyring analysis show the crucial involvement of water molecules both in the transformation of allylic alcohol into a ketone as well as in the concomitant isomerization of the exo-coordinated substrate into the *endo*-conformer. DFT structure and bonding analyses are used to assess the relative stabilities of the isomers and how the metal drives the electronic distribution on the substrate.

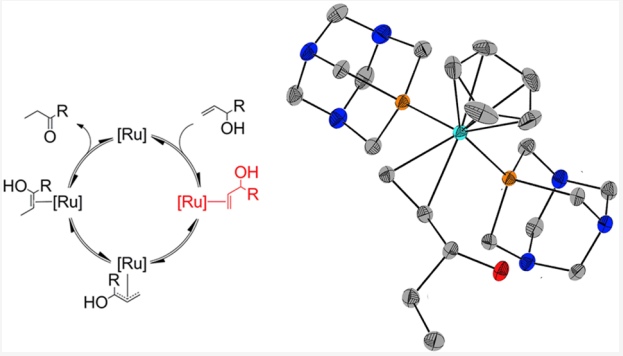

INTRODUCTION

The isomerization of allylic alcohols catalyzed by metal complexes is an efficient procedure (100% atom economy) to obtain carbonyl compounds. Although the majority of these reactions are carried out in organic solvents, they can also occur in water and under mild conditions.[1−4]

Catalytic processes in water have considerable advantages in the chemical industry over competing similar processes based on organic solvents: Water is abundant, cheap, readily available, stable, and it has no environmental impact. However, most of the known reactive catalytic metal complexes are insoluble in water or decompose when dissolved in it. In previous work, we have shown how water-soluble ruthenium complexes can achieve the isomerization of allylic alcohols in water under mild conditions[5−8] and how water influences in a crucial way some of these reactions.[9] For the isomerization of allylic alcohols, three main mechanisms have been proposed in the literature (Scheme 1): (a) the metal hydride addition−elimination mechanism, or alkyl mechanism; (b) the π-allyl metal hydride or η^3-allyl mechanism; and (c) the enone mechanism that invokes the metal oxygen coordination.[10−13] None of these mechanisms explicitly involve the participation of solvent molecules in the process.

Despite some catalysts being shown to require the presence of a base, including water, to stabilize specific intermediates during the catalytic cycle,[13−15] we have developed metal complexes that catalyze this reaction just in water.

In particular, our work has shown that the isomerization of linear allylic alcohols from propenol to octenol catalyzed by $[RuCp(H_2O\text{-}\kappa O)(PTA)_2](CF_3SO_3)$ (**1CF$_3$SO$_3$**) (PTA = 1,3,5-triaza-7-phosphaadamantane) has distinctive peculiarities with respect to previously published results: (a) No ligand loss is observed during the reaction, which suggests that the mechanism is somewhat different from those previously

Scheme 1. Proposed Mechanisms for the Catalytic Isomerization of Allyl Alcohols[a]

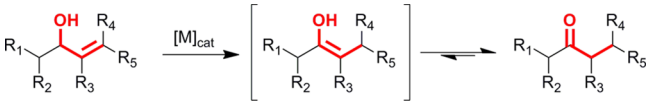

[a]Mechanisms: (a) alkyl mechanism; (b) η^3-allyl mechanism; (c) enone mechanism.

Received: September 2, 2020
Published: December 8, 2020

https://dx.doi.org/10.1021/acs.organomet.0c00585
Organometallics 2020, 39, 4491−4499

proposed (Scheme 1). (b) A large amount of water (far more than the stoichiometric amount) is required for the reaction to take place. (c) The minimum amount of water needed to reach the highest yields differs for each substrate.[9]

We presented a method for working out how many water molecules interact with the noncatalytic precursor [RuCp-$(PTA)_2$-μ-CN-1κC:2$\kappa^2 N$-RuCp$(PTA)_2$](CF_3SO_3).[16] Our approach was based on a combination of neutron scattering experiments, semiempirical atomistic calculations,[17] and *ab initio* molecular dynamics (AIMD) simulations. In the case of this catalytic precursor, we could identify important interactions between water molecules and N_{PTA} atoms, as well as with the lipophilic Cp ligand. Due to the large recording time and high concentrations required by neutron scattering techniques, we first studied by our procedure the isomerization of 1-propen-3-ol in water catalyzed by **1**CF_3SO_3 (Scheme 2), which is a very slow reaction. During this reaction,

Scheme 2. Structure of 1CF_3SO_3

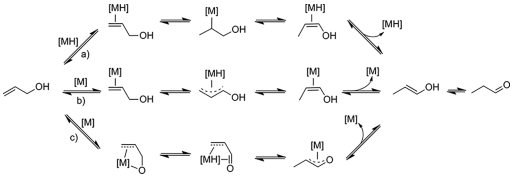

the only detectable complex in solution was found to be $[RuCp(exo\text{-}\eta^2\text{-}CH_2{=}CH{-}CH_2{-}OH)(PTA)_2]^+$, which is stable enough to permit a full characterization in water solution by means of neutron scattering and NMR. Furthermore, AIMD simulations reveal the existence of a chain composed of three hydrogen-bonded water molecules linking the alcohol to the PTA ligand and stabilizing the complex in its *exo*-conformation.[18] Despite these interesting findings, the water-assisted isomerization mechanism of linear allylic alcohols catalyzed by complex **1**CF_3SO_3 remains, at present, largely obscure.

To provide some insight into this question, we investigate the isomerization of allylic alcohols larger than 1-propen-3-ol catalyzed by **1**CF_3SO_3. Particularly, we concentrate our efforts to study the isomerization of 1-penten-3-ol into diethyl ketone. In contrast with the isomerization of 1-propen-3-ol, the reaction with 1-penten-3-ol occurs at 55 °C in minutes when the water content is above 50 equiv with respect to the substrate.[9] In this paper we present the study by NMR of this reaction and the full characterization of the catalytic reaction intermediate $[RuCp(\eta^2\text{-}1\text{-penten-3-ol})(PTA)_2]^+$ (**2**) by single-crystal X-ray diffraction as well as by DFT bonding analysis. To the best of our knowledge, this is the first crystal structure for an allylic isomerization reaction and the first crystal structure of a water-soluble metal complex containing a coordinated allylic alcohol. Furthermore, in our NMR studies we show how water influences the dynamics of the complex prior to the catalytic process.

RESULTS AND DISCUSSION

Crystal Structure of $[RuCp(PTA)_2(exo\text{-}\eta^2\text{-}CH_2{=}CHOH{-}CH_2{-}CH_3)](CF_3SO_3)\cdot 2H_2O$ (*exo*-2$CF_3SO_3\cdot 2H_2O$). A concentrated solution of the product obtained from the reaction of **1**CF_3SO_3 with 1-penten-3-ol in water/EtOH (1:10) provided single crystals of ***exo*-2$CF_3SO_3\cdot 2H_2O$** suitable for X-ray crystal structure determination. The crystal structure of the complex is shown in Figure 1 and selected interatomic distances and angles are given in the figure caption (for more details, see the Supporting Information).

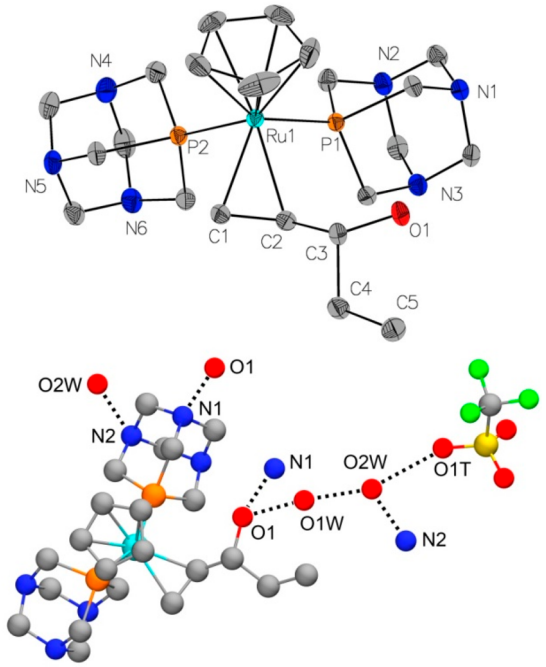

Figure 1. Top: Crystal structure of ***exo*-2$(CF_3SO_3)\cdot 2H_2O$**. Selected distances and angles: Ru1−P1 = 2.3038(7) Å; Ru1−P2 = 2.2929(7) Å; Ru1−C1 = 2.214(3) Å; Ru1−C2 = 2.239(3) Å; (C1−C2 = 1.396(4) Å), C2−C3 = 1.509(4) Å; O1−C3 = 1.438(3) Å; Ru−Cp_{cent} = 1.886 Å; P2−Ru1−P1 = 93.12(3)°. Bottom: hydrogen bond network around ***exo*-2$(CF_3SO_3)\cdot 2H_2O$**. Hydrogen atoms have been omitted for clarity.

In the complex unit, the Ru atom is coordinated with a distorted pseudo-octahedral geometry by one η^5-Cp, two PTA ligands through the P atom, and one η^2-CH=CH coordinated 1-penten-3-ol. It is important to stress that complex ***exo*-2$CF_3SO_3\cdot 2H_2O$** is the first crystallized example of a metal complex containing a coordinated allylic alcohol[19] and the first crystallized reaction intermediate involving allylic alcohols.[19]

The unit cell contains two *exo*-η^2-$CH_2{=}CH_2$ complexes related by an inversion center, with the $CH(OH)CH_3$ group in opposite direction relative to the $\{CpRu(PTA)_2\}^+$ moiety (Figure 1). The metal displays a distorted pseuo-octahedral coordination sphere with the angle P−Ru−P (P2−Ru1−P1 = 93.12(3)°) within the range observed in similar ruthenium complexes.[19] Nevertheless, this angle is notably smaller than those of starting aqua complex **1** (P2−Ru1−P1 = 95.47(2)°) and chloride complex $[RuClCp(PTA)_2]$ (P2−Ru1−P1 = 96.18(7)°). The Ru−P bonds (Ru1−P1 = 2.3038(7) Å; Ru1−P2 = 2.2929(7) Å) are also in the range found for similar compounds,[19] being larger than those found in **1**CF_3SO_3 (Ru1−P1 = 2.2654(10) Å; Ru1−P2 = 2.2614(8) Å) and those found in the chloride complex $[RuClCp(PTA)_2]$ (Ru1−P1 = 2.2525(18) Å). The Ru−Cp_{cent} distance (1.886 Å) is larger than that in **1**$CF_3SO_3\cdot 2H_2O$ (1.837 Å), but it remains within the range of bond lengths listed in the literature (1.836−1.929 Å; mean 1.868 Å).[19] Both Ru−C bond lengths (Ru1−C1 = 2.214(3) Å; Ru1−C2 = 2.239(3) Å) are larger than the Ru−OH_2 bond in starting complex **1** (Ru−O = 2.1784(16) Å) but in the range of those in crystal structures of

https://dx.doi.org/10.1021/acs.organomet.0c00585
Organometallics 2020, 39, 4491−4499

ruthenium complexes containing η^2-C=C groups[19] as well as the C=C (C1−C2 = 1.396(4) Å). The remaining distances and angles are all within the ranges found for similar compounds. Complexes are involved in an extended network of hydrogen bonds (Figure 1) with distances larger than 2.5 Å, which are consistent with weak hydrogen bonds,[20] the shortest distance being O1−O1W (2.548(18) Å).

Study of the Reactivity of 1-Penten-3-ol against $1CF_3SO_3$: Synthesis and NMR Characterization of 2. Reaction of $\mathbf{1CF_3SO_3}$ with 20 equiv of 1-penten-3-ol in D_2O or in MeOD/D_2O 5:1 at room temperature was studied with $^{31}P\{^1H\}$ NMR spectroscopy, which shows four doublets starting to appear after 10 min and persist for at least 20 h (D_2O: −21.6, −24.5, −22.2, and −24.1 ppm; CD_3OD/D_2O: −22.44, −25.60, −22.97, and −24.85 ppm). The ^1H NMR spectrum also shows the presence of excess 1-penten-3-ol and 3-pentenone, but the isomerization process is very slow (TOF = 0.7 h^{-1}). Running the same reaction in dry MeOD leads to the precipitation of a white powder, whose $^{31}P\{^1H\}$ and ^1H NMR spectra in solution are similar to those obtained in MeOD/D_2O 5:1, where no precipitate was observed.

This white compound is found to be insoluble in organic solvents, whereas it readily dissolves in D_2O, where it displays a $^{31}P\{^1H\}$ NMR containing the same number of signals and chemical shifts as those observed in reactions of $\mathbf{1CF_3SO_3}$ with 1-penten-3-ol studied with NMR. After 12 h at room temperature, partial decomposition of the product is observed, and a singlet at 24.95 ppm appears which is ascribable to catalyst complex **1**. The $^{13}C\{^1H\}$ NMR spectrum showed that the decomposition is also followed by the release of 3-pentanone. In order to study this transformation, NMR spectra at lower temperature were measured in MeOD/D_2O (5:1), to avoid the freezing of the sample. In this solvent and at 273 K, the decomposition of the complex is kept up at least 3 days, and the $^{31}P\{^1H\}$ NMR shows the appearance of two AB systems in a 5.4:1 rate, consistent with a mixture of two different $[RuCp(\eta^2\text{-1-penten-3-ol})(PTA)_2]^+$ complex isomers (Scheme 3). These species were further studied using ^1H, $^1H-^1H$ COSY, and selective 1D-TOCSY NMR.

Scheme 3. Synthesis of 2

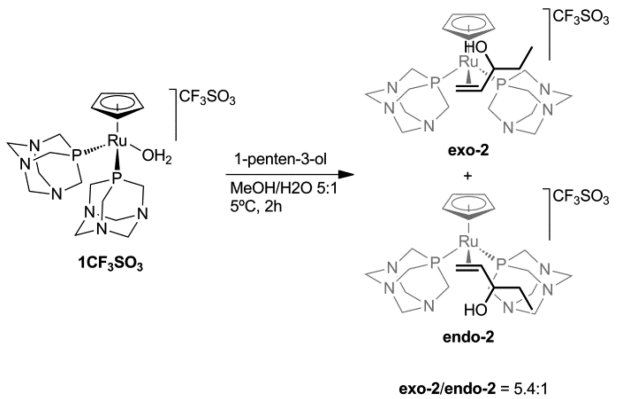

For both the observed isomers, ^1H NMR revealed that there are some differences in the chemical shifts of the allylic alcohol ligand, larger differences being observed for the alkene H3, H1a, and H1b protons (Figure 2; see the Supporting Information). Unfortunately, the minority species' α-CH (3.85 ppm) is responsible for the only signal that does not overlap with others. Analysis of the ROESY map made it possible to study the conformation of the major species: Its H1a (3.01 ppm) and H3 (2.87 ppm) signals are coupled in space with the Cp protons, which agrees with an *exo*-conformation (***exo*-2**) of the coordinated allylic alcohol. This is similar to what has been observed in $[RuCp(exo\text{-}\eta^2\text{-}CH_2{=}CH{-}CH_2{-}OH)(PTA)_2]^+$, although in the latter case only the *exo*-isomer was identified in solution.[18] The NMR characterization of ***exo*-2** in MeOD/D_2O (5:1) at 273 K shows that in the ^1H and $^{13}C\{^1H\}$ spectra the singlet of the Cp and the multiplets of the PTA appear in the regions expected for a ruthenium piano-stool complex (^1H: Cp = 5.37 ppm, PTA = 4.07−4.82 ppm; $^{13}C\{^1H\}$: PTA: PCH_2N = 54.6 ppm, 55.6 ppm; PTA: NCH_2N = 71.5 ppm). Peaks corresponding to the pentenol ligand are spread between 1.02 and 3.05 ppm in the ^1H spectrum and between 9.68 and 78.79 ppm in the $^{13}C\{^1H\}$ spectrum. These signals are due to the allylic alcohol group, similar to what was found for $[RuCp(exo\text{-}\eta^2\text{-}CH_2{=}CH{-}CH_2{-}OH)(PTA)_2]^+$ (^1H: H1a = 3.01 ppm, H1b = 2.00 ppm, H2 = 2.81 ppm, H3 = 2.87 ppm; $^{13}C\{^1H\}$: C1 = 31.2 ppm, C2 = 63.9 ppm, C3 = 78.8 ppm).[18] The $^{31}P\{^1H\}$ NMR spectrum displays two doublets corresponding with two chemically different PTA ligands, which appears at −22.4 ppm and −25.6 ppm ($^2J_{PP}$ = 42.4 Hz). Unfortunately, in the routine NMR experiments the key cross peaks corresponding to the minority species could not be separated.

In order to find experimental support to elucidate the structure of the minor species, a 3D TOCSY-ROESY of the solution of the white precipitate in a mixture of MeOD/D_2O (5:1) at 273 K was recorded. In a TOCSY-ROESY experiment, when a ROE transfer of the magnetization occurs after spin−lock, a cross peak is generated on a line parallel to the F3 dimension, while TOCSY is observed along F1. It is important to point out that for each ROE peak the corresponding spin−lock pattern appears in F1. In Figure 2 the F1/F3 plane perpendicular to the Cp resonance (5.3 ppm) in F2 is shown. While ROE due to ***exo*-2** is evident, cross peaks relative to the minority species can also be singled out from the mixture. The analysis of these cross peaks indicates that Cp protons are spatially close to H1b (3.15 ppm) and H2 (3.05 ppm), which is only possible if in solution the minor species corresponds to the isomer $[RuCp(endo\text{-}\eta^2\text{-1-penten-3-ol})(PTA)_2]^+$ (***endo*-2**). It is important to stress the fact that when reaction of $\mathbf{1CF_3SO_3}$ with 1-propen-3-ol was studied only the formation of complex $[RuCp(exo\text{-}\eta^2\text{-1-propen-3-ol})(PTA)_2]^+$ was observed.[18]

Comparison of the chemical shifts for both isomers reveals that the alkene protons Ha and Hb of ***endo*-2** (H1b = 3.15 ppm; H2 = 3.05 ppm; H1a = 1.99 ppm) are inverted with respect to those of isomer ***exo*-2** (H1a = 3.01 ppm; H1b = 2.00 ppm; H2 = 2.81 ppm) and $[RuCp(exo\text{-}\eta^2\text{-1-propen-3-ol})(PTA)_2]^+$ (H1a = 2.98 ppm; H1b = 2.01 ppm; H2 = 2.80 ppm). Therefore, flipping the allylic alcohol ligand around the double bond axis affects the chemical shift of Ha and Hb, but it does not seem to affect H2 appreciably. Other analogies with $[RuCp(exo\text{-}\eta^2\text{-1-propen-3-ol})(PTA)_2]^+$ can also be found: Its β-CH_2 protons H3 and H3′ appear at 3.05 and 3.92 ppm, respectively, while for ***endo*-2** they appear at H3 = 3.85 ppm and for ***exo*-2** at H3 = 2.87 ppm. In ***endo*-2** as well as in ***exo*-2** hydrogen H3 points toward the Cp, which indicates that in both conformers the alcohol is oriented in the opposite direction.

Variable-temperature $^{31}P\{^1H\}$ NMR studies run in the range of 193−273 K in CD_3OD/D_2O (5:1) and in the range of 293−

https://dx.doi.org/10.1021/acs.organomet.0c00585
Organometallics 2020, 39, 4491−4499

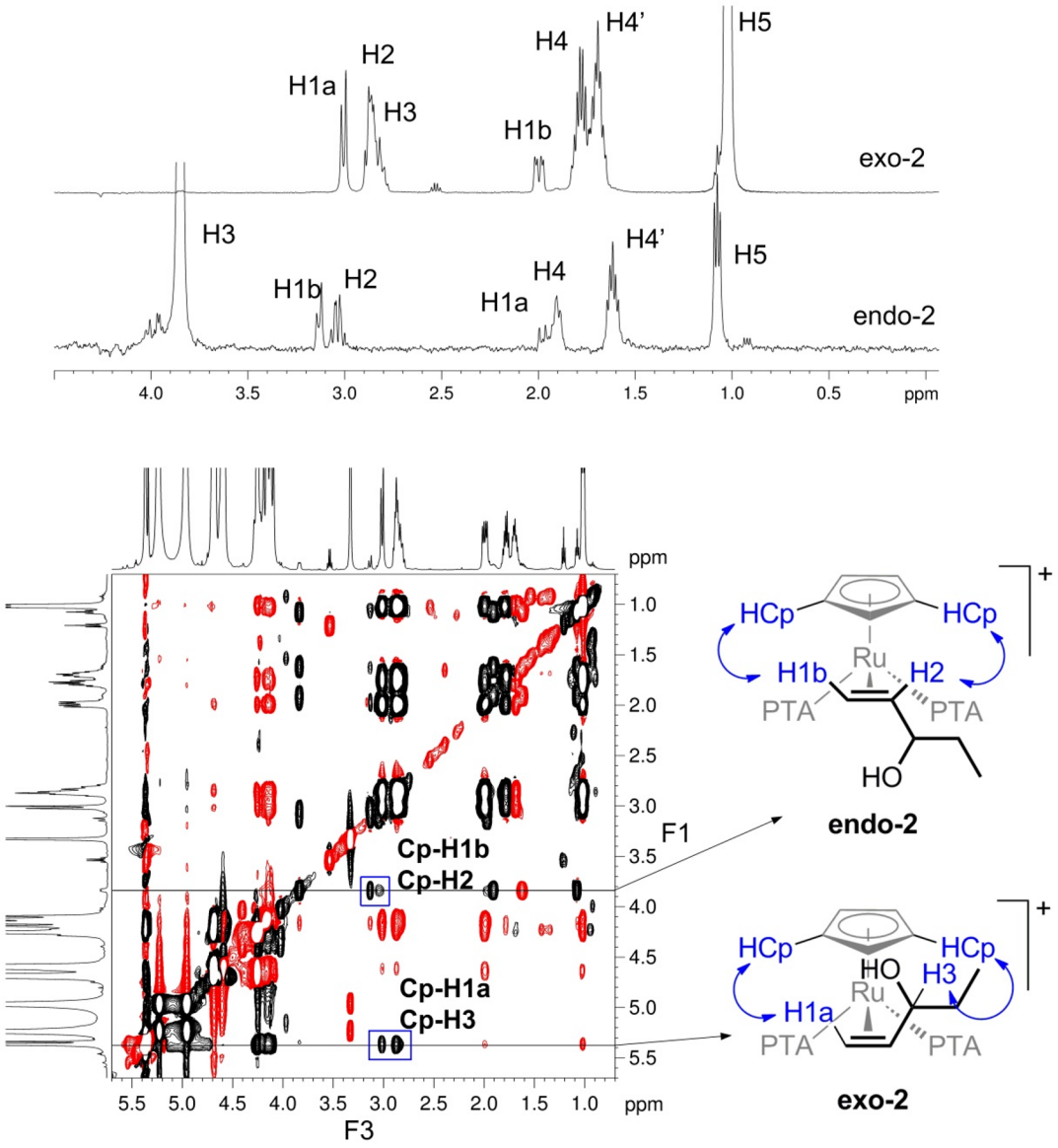

Figure 2. NMR separation of the isomers of **2**. Top: stacked selective 1D TOCSY spectra of **2** in CD_3OD/D_2O 5:1 at 273 K irradiated at 1.02 ppm (***endo*-2**) and 2.85 ppm (***exo*-2**). Bottom: F1F3 plane of a 3D TOCSY-ROESY of **2** in CD_3OD/D_2O 5:1 at 273 K through the resonance position of the Cp ligand (5.34 ppm). The different spin−lock patterns of ***exo*-2** and ***endo*-2** permit to identify the key ROE interactions Cp-H1a, Cp-H3 (***exo*-2**) and Cp-H1b, Cp-H2 (***endo*-2**) along the ROE-lines parallel to F3.

353 K in D_2O show that the *exo*- and *endo*-isomers are in an equilibrium. Unfortunately, at 193 K the coalescence of the peaks is incomplete, and from 223 K only broad signals are observed. Interestingly, if the NMR solution is cooled in liquid N_2 and measured at 273 K immediately after melting, then ***exo*-2** is the unique species observed.

The study of the *exo*−*endo* isomerization of **2** through Eyring analysis (Figure 3) revealed that the interconversion of the isomers of **2** requires and is strongly influenced by water. Entropy differences suggest that both forward and backward isomerization are multimolecular processes: For k_b, they are negative in both solvent systems and agree with a molecular disaggregation. In contrast, for k_f a negative and heavier entropic contribution is found in CD_3OD/H_2O 5:1 ($\Delta S^{\ddagger} = -2.70 \times 10^{-2} \pm 0.1 \times 10^{-2}$ kcal/K·mol), while in D_2O it is positive and lower in absolute magnitude ($\Delta S^{\ddagger} = 2.7 \times 10^{-3} \pm 0.36 \times 10^{-3}$ kcal/K·mol), that agrees with a disaggregation in the first case and an aggregation in the latter. This behavior could arise from disruption and formation of structured water frameworks around the complex,[18] which should be more probable when isomerization occurs in pure water. The activation enthalpy for k_f is higher in D_2O than in CD_3OD/H_2O 5:1, while for k_b it is negative in both solvent systems. Previous reports suggest that negative activation enthalpies could be related to non-covalent interactions or entropic factors affecting the reaction.[21] For the forward reaction, the entropy differences in the studied solvents are the factors that lead to a higher overall activation barrier at 273 K when isomerization occurs in CD_3OD/H_2O (5:1) (D_2O: $\Delta G^{\ddagger} = 3.71 \pm 0.22$; CD_3OD/H_2O (5:1): $\Delta G^{\ddagger} = 10.16 \pm 0.51$ kcal/mol) (Table S5). Another aspect that can be observed from the distribution of the kinetic constants k_f and k_b as a function of temperature is that in D_2O k_f is higher than k_b above 289.8 K. This means that, from this temperature, the isomerization of ***exo*-2** to ***endo*-2** is faster than the backward reaction. In CD_3OD/D_2O (5:1) this behavior is observed at a much higher

https://dx.doi.org/10.1021/acs.organomet.0c00585
Organometallics 2020, 39, 4491−4499

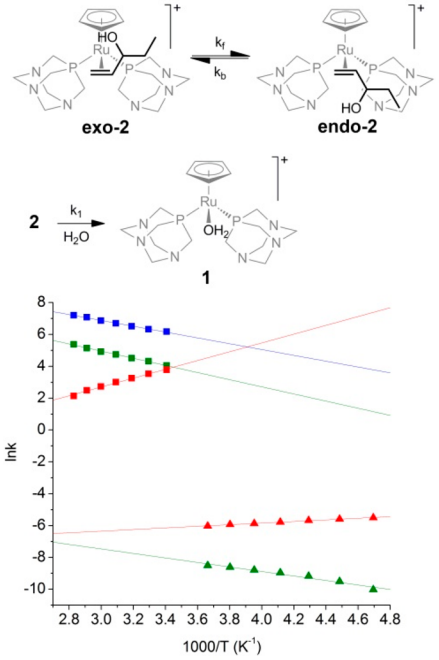

Figure 3. Eyring plots for k_f, k_b, and k_1 in D_2O and for k_f and k_b in MeOD/D_2O 5:1. Slope = $-\Delta H^{\ddagger}/R$. Intercept = $\Delta S^{\ddagger} + \ln(k_b/h)$.

temperature, as the k_f and k_b intercept at 413.6 K. Finally, the decomposition of **2** into **1** and pentanone is always faster than the *exo*−*endo* isomerization.

To investigate the hypothesis that the evolution of **2** into **1** is strongly influenced by water, we changed the triflate anion with the more lipophilic BAr^F to obtain [RuCp(η^2-1-penten-3-ol)$(PTA)_2$]BAr^F (**2BAr^F**) (BAr^F = tetrakis[3,5-bis-(trifluoromethyl)phenyl]borate), which is soluble in organic solvents, by reacting [RuClCp$(PTA)_2$] with 1-penten-3-ol and $NaBAr^F$ in dry THF. The $^{31}P\{^1H\}$ NMR spectrum of **2BAr^F** in dry acetone-d_6 displays only signals corresponding to the *endo*- and *exo*-isomers of **2**, without showing decomposition during at least 15 h at room temperature. Titration with D_2O conducted on a solution of **2** in acetone-d_6 leads to the formation of **1** and 3-pentanone, together with the consumption of ***endo*-2** (Figure S15).

DFT Structure and Bonding Analysis of 2. Bond lengths and dihedral angles of the B3LYP/def2-TZVPP calculated geometries of ***exo*-2** in gas phase and implicitly described aqueous solvent are given along with the crystal structure values in Table S1. The overall agreement between the three structures is good. In the respective conformation (corresponding to the crystal structure in Figure 1), the substrate 1-penten-3-ol in its *R* stereoisomer coordinates to the ruthenium complex in the *exo*-conformation, with the hydrogen H3 pointing toward the cyclopentadienyl ring (in the following referred to as *exo*(a)-conformation). This *exo*(a)-conformation corresponds to the structure postulated in our previous work[18] on the same reaction of ruthenium complex **1CF$_3$SO$_3$** with 1-propen-3-ol in aqueous solution. In this occasion, we were not able to obtain the crystal structure of this intermediate species, and we thus determined its molecular structure using NMR data, DFT geometry optimizations and AIMD (*ab initio* molecular dynamics) simulations. However, at variance with 1-propen-3-ol, the substrate 1-penten-3-ol is chiral, owing to the presence of a substituted CH_2CH_3 moiety at C3. The number of potential local minima for the rotation of the C2−C3 bond and the potential arrangements of the alkene double bond coordinated to ruthenium is therefore larger. In Table 1, we list a total of five *exo*- and five *endo*-conformers of **2** that we found to be local minima on the potential energy surface. For *exo*(a−d)/*endo*(a−d), the *endo*-structures correspond to the rotation around the C2═C3 bond of the respective *exo*-structure. Conformer *exo*(a) is indeed the lowest in energy compared to the other local minimum conformers. The latter and the second lowest *exo*-isomer (*exo*(d) ΔE = 2.4 kcal/mol) both have the bulky CH_2CH_3 moiety pointing away from the complex center. In general, we observe a tendency for the *endo*-

Table 1. Comparison of Different *exo*- and *endo*-Conformers of 2[a]

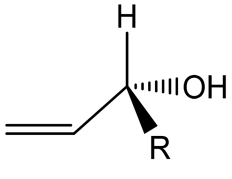	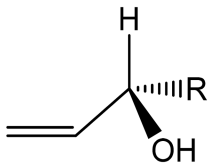	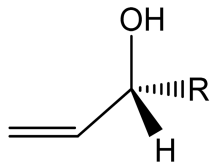	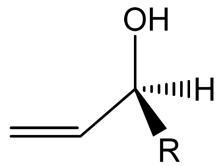	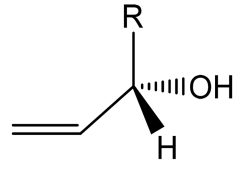
exo(a)	exo(b)	exo(c)	exo(d)	exo(e)
0.0 kcal/mol	6.4 kcal/mol	4.2 kcal/mol	2.4 kcal/mol	4.5 kcal/mol
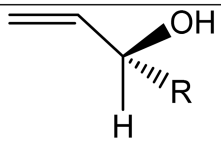	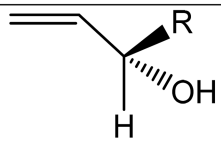	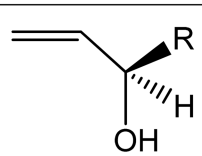	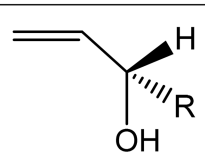	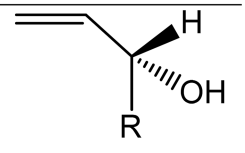
endo(a)	endo(b)	endo(c)	endo(d)	endo(e)
12.1 kcal/mol	4.4 kcal/mol	4.4 kcal/mol	9.0 kcal/mol	8.8 kcal/mol

[a]Ruthenium complex located behind the paper plane (behind the C1═C2−C3 moiety) and with the cyclopentadienyl ligand pointing up not displayed.

https://dx.doi.org/10.1021/acs.organomet.0c00585
Organometallics 2020, 39, 4491−4499

structures to be at higher energies (4.4−12.1 kcal/mol higher than *exo*(a)) compared to the *exo*-conformers (2.4−6.4 kcal/mol higher than *exo*(a)). This corresponds to the experimental findings of the Eyring analysis that shows a preference for the backward reaction from the *endo*- to the *exo*-conformer at low temperatures. Again, in the two lowest structures *endo*(b) and *endo*(c) with each 4.4 kcal/mol above *exo*(a) the CH_2CH_3 residue is facing away from ruthenium. In direct comparison with *exo*(a) the structure *endo*(b) is a rotational isomer where the substrate is rotated by approximately 180° around the η^2-Ru-(C1═C2) bond. Structure *endo*(c) could potentially be obtained by either rotation around the C1═C2 or a flip of the whole substrate followed by a rotation around the C2−C3 single bond.

Examination of the frontier orbitals of ***exo*-2** in Figure S18 shows that the lowest four occupied orbitals consist of hybrid orbitals of the PTA ligand orbitals and several d orbitals at ruthenium, while the two highest unoccupied orbitals exhibit electron density at the aromatic cyclopentenyl ring and at the ruthenium center. This is similar (although less well-defined) to what we previously observed in a study of octahedral ruthenium complexes with PTA and aromatic η^1(N) bipyridyl ligands.[22] Consistent with the findings of this work, the NBO charge analysis given in Table 2 shows that the formally

Table 2. NBO Charges for *exo*-2 at B3LYP/def2-TZVPP[a]

	[Ru][a]	1-penten-3-ol
Ru	−0.180	
Cp	0.089	
PTA1	0.542	
PTA2	0.543	
1-penten-3-ol	0.006	0
C1	−0.412	−0.389
C2	−0.216	−0.157
C3	0.075	0.057
H1a	0.213	0.183
H1b	0.204	0.197
H2	0.212	0.192
H3	0.156	0.156

[a][Ru] = $[RuCp(1\text{-penten-3-ol})(PTA)_2]^+$. All values in e

negatively charged cyclopentadienyl ring overall donates over one electron to ruthenium and has a small final positive charge of 0.089 e. Further net donation of two half electrons from each of the PTA ligands leads to a negative charge of −0.180 e at Ru, reversing the charge sign of the formally positively charged transition metal ion.

There is virtually no net electron density shift between the 1-penten-3-ol substrates and the complex as the NBO net charges at the substrate within the complex are close to zero. This does not imply that the coordination of the substrate to the metal center is weak, as it is well-known for alkene η^2-complexes, that there is indeed electron density transferred in both directions, namely, from the substrate into empty orbitals at the metal center and vice versa.[23] The charge distribution within the 1-penten-3-ol does change as a result of the coordination to the complex, as the negative charges at C1 (−0.412 e) and C2 (−0.216 e) decrease slightly in the ruthenium complex relative to the free substrate (q_{C1} = −0.389 e, q_{C2} = −0.157 e), which is balanced by an increase of the positive charges at the substrate hydrogen atoms. Indeed, the only positively charged carbon atom in 1-penten-3-ol is C3, which promotes the proton abstraction in the catalytic transformation of allyl alcohols into aldehydes and ketones.[18] This positive charge increases on coordination to the ruthenium center, although this change is minimal and thus potentially not the decisive factor in the proton abstraction step.

Table 3 and Figures 3, S18, and S19 give the results of the EDA-NOCV analysis of ***exo*-2** with fragments (a) [RuCp-

Table 3. EDA-NOCV Analysis of *exo*-2 at B3LYP/TZ2P[a]

	[Ru] and 1-penten-3-ol	[Ru] and Cp^-	[Ru] and PTA
ΔE_{int}	−47.7	−267.1	−48.5
ΔE_{Pauli}	156.9	232.5	155.0
ΔE_{elstat}	−116.8 (57.1%)	−316.2 (63.3%)	−126.4 (62.1%)
ΔE_{orb}	−87.8 (42.9%)	−183.5 (36.7%)	−77.1 (37.9%)

[a][Ru] = $[RuCp(1\text{-penten-3-ol})(PTA)_2]^+$. All energies in kcal/mol. The values in parentheses give the percentage contribution to the total attractive interactions $\Delta E_{elstat} + \Delta E_{orb}$.

$(PTA)_2]^+$ and 1-penten-3-ol, (b) $[Ru(1\text{-penten-3-ol})(PTA)_2]^{2+}$ and Cp^-, and (c) $[RuCp(1\text{-penten-3-ol})(PTA)]^+$ and PTA. The interaction energy ΔE_{int} between the complex and the cyclopentadienyl fragment (−267.11 kcal/mol) is considerably higher than in case of of 1-penten-3-ol (−47.70 kcal/mol) and PTA (−48.54 kcal/mol), which are very similar (even if the abstraction of the phosphine ligands could not be observed experimentally). Among the attractive contributions, it is in all cases the electrostatic energy ΔE_{elstat} that plays the dominant role (ca. 60%). At first sight, this finding appears to be in disagreement with the results of Caramori et al.[24] on similar ruthenium complexes with three NH_3 and one η^6-coordinated [2.2]paracyclophane ligand (which consists of two ethyl bridged benzenes), in which the electrostatic contribution only amounts to 42%. However, in the latter complex the aromatic ligand is neutral, and if the aromatic ligand is protonated at its peripheric second benzene ring, then the value of ΔE_{elstat} further decreases to 15.4%, which supports the existence of a trend of decreasing electrostatic contribution with increasing ligand charges.

Consistent with the NBO results, in the orbital interaction of cyclopentadienyl with the remaining complex (Figure S19), the first three deformation densities $\Delta\rho_{1-3}$ (amounting for 74.2% of the orbital energy) indicate an electron donation from different occupied cyclopentadienyl orbitals to ruthenium. PTA exhibits strong σ-donation ability (amounting for 65.4% of the orbital energy) and only moderate π back-donation from two orthogonal electron-accepting p orbitals on phosphorus (adding up to a total of 23.6% of the orbital energy), similar to what has been observed for other phosphine ligands.[25] Direct comparison with the interaction in the presence of the 1-penten-3-ol fragment (Figure 3) shows that this situation is reversed in the allylic alcohol, where it is indeed the π back-donation from a d orbital at ruthenium into the C1═C2 antibonding π orbital that accounts for nearly half of the fragment interaction. The latter may benefit from the large amount of electron density that is donated toward ruthenium from the Cp and the PTA ligands.

The only other significant contribution arises from the σ-donation from the C1═C2 bonding π orbital to ruthenium, which is however decidedly less pronounced (ca. 36.7%). Other contributions are at least one order of magnitude lower, but the symmetrized fragment orbital (SFO) from the EDA-

https://dx.doi.org/10.1021/acs.organomet.0c00585
Organometallics 2020, 39, 4491−4499

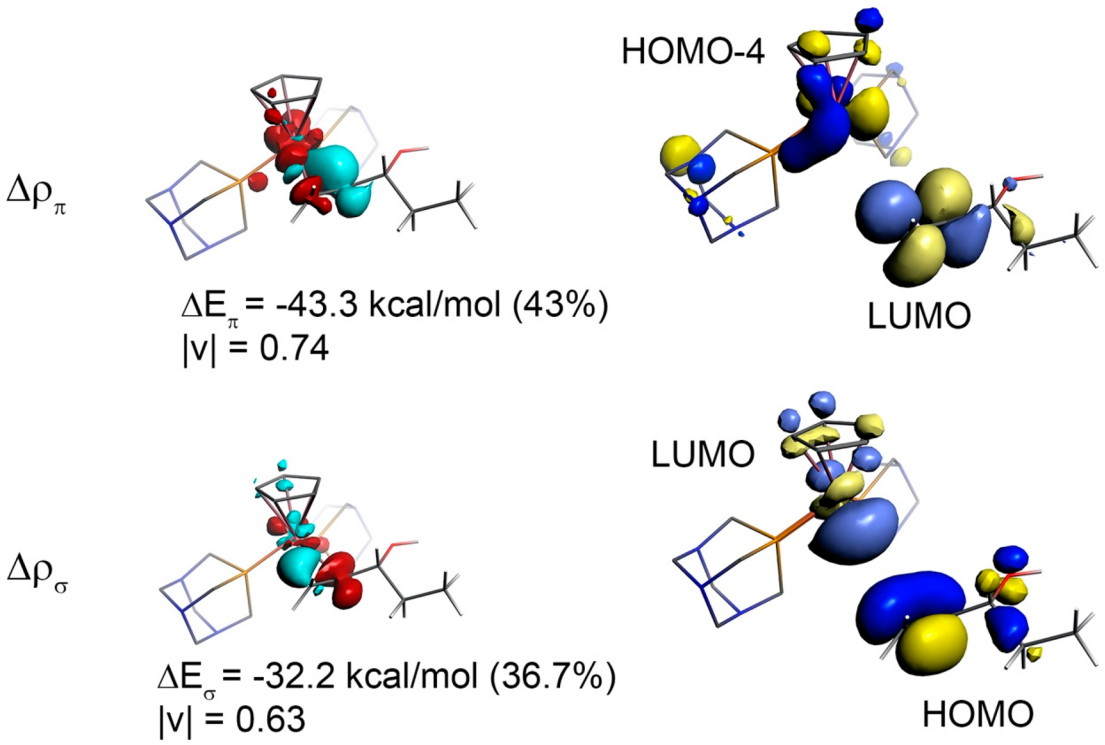

Figure 4. EDA-NOCV of ***exo*-2** with fragments $[RuCpPTA_2]^+$ and 1-penten-3-ol calculated with B3LYP/TZ2P. The values in parentheses give the percentage contribution to the total orbital interactions ΔE_{orb}, and $|v|$ corresponds to the eigenvalue. Electron density flow is from red to blue.

NOCV contributions predominantly indicate further electron donation from 1-penten-3-ol to the complex.

With respect to the C1═C2 double bond, both the donation of electron density from the π-bonding orbital and the back-donation into the π-antibonding orbital have a C═C bond-weakening effect. This is also reflected in the Wiberg bond indices (Table S4) that show a decrease in bond order going from isolated 1-penten-3-ol (1.97) to the respective C1═C2 bond in ***exo*-2** (1.41). This reduction in bond order from a genuine double bond to between a single and a double bond could facilitate an isomerization from the *exo*-isomer to the *endo*-isomer by rotation around the C1═C2 bond in the coordinated complex. Alternatively, purely rotational isomerization mechanisms by either rotation around the η^2-Ru−(C1═C2) bond or vertical flipping of the substrate along the C1═C2 bond would decrease the orbital overlap of the π back-donation between the complex HOMO−4 and the substrate LUMO (Figure 4, top) and thus energetically disfavor a direct isomerization process. In fact, vertical flipping would additionally lead to a decrease in orbital overlap, considering the presence of a σ donation from the substrate HOMO to the complex LUMO.

Other mechanistic possibilities for the isomerization can be the induction of a first reaction step (e.g., according to isomerization mechanisms shown in Scheme 1) or a full or partial dissociation of the substrate followed by a reattachment in the *endo*-conformation. Water molecules present in the complex vicinity might play a role in altering the electronic structure of ***exo*-2** and induce isomerization by one of the described mechanisms. We will explore the isomerization process in more detail elsewhere.

CONCLUSION

With $[RuCp(exo\text{-}\eta^2\text{-}1\text{-penten-3-ol})(PTA)_2](CF_3SO_3)\cdot 2H_2O$, we present the first crystal structure of a metal complex containing a coordinated allylic molecule and the first crystal structure of a water-soluble complex containing a η^2-C═C group. In contrast to our previous studies, we find that in solution and only in the presence of water it is not only the catalytic isomerization to the ketone that is taking place but also the isomerization from the *exo*- to the *endo*-coordinated conformer. Eyring analysis shows that the catalytic transformation to pentanone is favored over the formation of the *endo*-isomer, but the equilibrium between the *exo*- and *endo*-coordination is shifted toward the *endo*-isomer at room temperature. Overall, the isomerization to the *endo*-conformer becomes more favorable at higher temperatures and when the reaction occurs in pure water than in $MeOH/H_2O$ 5:1 mixture. Our calculations indicate that both the *exo*- and *endo*-conformers are stabilized if the CH_2CH_3 moiety is rotated away from the complex center. Bonding analysis shows that both the cyclopentadienyl and the PTA ligands effectively donate electron density to ruthenium. Consequently, the π back-donation of electrons from ruthenium into the empty C1═C2 π-antibonding LUMO orbital of 1-penten-3-ol is the strongest interaction in the coordination. This leads to a weakening of the C1═C2 double bond which can facilitate rotation and thus isomerization to the *endo*-conformer. We propose that the catalytic transformation from allylic alcohols to ketones in these complexes either happens via the formation of the *endo*-conformer prior to ketone formation or, alternatively, via an intermediate reaction step from which the formation of the *endo*-conformer and ketone formation occur along competing pathways. Therefore, this study goes ahead in the understanding on the role of water in Ru-driven

https://dx.doi.org/10.1021/acs.organomet.0c00585
Organometallics 2020, 39, 4491−4499

isomerization catalysis, potentially solving a long-standing mechanistic issue, which has been addressed in the literature but not conclusively resolved. We will examine the underlying mechanisms in further work and study in detail the involvement of water, which we have observed here to be an indispensable reagent in all of these reactions.

■ ASSOCIATED CONTENT

Supporting Information

The Supporting Information is available free of charge at https://pubs.acs.org/doi/10.1021/acs.organomet.0c00585.

Details on synthesis, NMR spectra, NBO charge and bond order analysis, and EDA-NOCV (PDF)

Accession Codes

CCDC 2015844 contains the supplementary crystallographic data for this paper. These data can be obtained free of charge via www.ccdc.cam.ac.uk/data_request/cif, or by emailing data_request@ccdc.cam.ac.uk, or by contacting The Cambridge Crystallographic Data Centre, 12 Union Road, Cambridge CB2 1EZ, UK; fax: +44 1223 336033.

■ AUTHOR INFORMATION

Corresponding Author

Antonio Romerosa − *Área de Química Inorgánica-CIESOL, Universidad de Almería, 04120, Spain;* orcid.org/0000-0002-6285-9262; Email: romerosa@ual.es

Authors

Franco Scalambra − *Área de Química Inorgánica-CIESOL, Universidad de Almería, 04120, Spain*

Belen Lopez-Sanchez − *Área de Química Inorgánica-CIESOL, Universidad de Almería, 04120, Spain*

Nicole Holzmann − *Research Center for Computer-Aided Drug Discovery, Shenzhen Institutes of Advanced Technology, Chinese Academy of Sciences, Shenzhen 518055, China; Scientific Computing Department, STFC Rutherford Appleton Laboratory, Harwell Oxford, Didcot OX11 0QX, United Kingdom;* orcid.org/0000-0001-5717-1984

Leonardo Bernasconi − *Center for Research Computing, University of Pittsburgh, Pittsburgh, Pennsylvania 15260, United States;* orcid.org/0000-0002-9460-7975

Complete contact information is available at: https://pubs.acs.org/10.1021/acs.organomet.0c00585

Author Contributions

The manuscript was written through contributions of all authors. All authors have given approval to the final version of the manuscript.

Funding

We thank the European Commission FEDER program for cofinancing the projects CTQ2015−67384-R (MINECO-Spain) and the PAI-research group FQM-317 (Junta de Andalucia-Spain). This research was supported in part by the University of Pittsburgh Center for Research Computing through the resources provided.

Notes

The authors declare no competing financial interest.

■ ACKNOWLEDGMENTS

N.H. and L.B. acknowledge support from the EPSRC Service Level Agreement with STFC Scientific Computing Department and computing resources provided by STFC Scientific Computing Department's SCARF cluster. N.H. thanks Prof. Gernot Frenking and the Theoretical Chemistry group of the Philipps-Universität Marburg for usage of computer time and licensed programs. This research was supported in part by the University of Pittsburgh Center for Research Computing through the resources provided.

■ REFERENCES

(1) Van Der Drift, R. C.; Bouwman, E.; Drent, E. Homogeneously Catalysed Isomerisation of Allylic Alcohols to Carbonyl Compounds. *J. Organomet. Chem.* **2002**, *650* (1−2), 1−24.

(2) Uma, R.; Crévisy, C.; Grée, R. Transposition of Allylic Alcohols into Carbonyl Compounds Mediated by Transition Metal Complexes. *Chem. Rev.* **2003**, *103* (1), 27−51.

(3) Cadierno, V.; Crochet, P.; Gimeno, J. Ruthenium-Catalyzed Isomerizations of Allylic and Propargylic Alcohols in Aqueous and Organic Media: Applications in Synthesis. *Synlett* **2008**, *2008*, 1105−1124.

(4) Ahlsten, N.; Bartoszewicz, A.; Martín-Matute, B. Allylic Alcohols as Synthetic Enolate Equivalents: Isomerisation and Tandem Reactions Catalysed by Transition Metal Complexes. *Dalt. Trans.* **2012**, *41* (6), 1660−1670.

(5) González, B.; Lorenzo-Luis, P.; Serrano-Ruiz, M.; Papp, É.; Fekete, M.; Csépke, K.; Osz, K.; Kathó, Á.; Joó, F.; Romerosa, A. Catalysis of Redox Isomerization of Allylic Alcohols by $[RuClCp(mPTA)_2](OSO_2CF_3)_2$ and $[RuCp(mPTA)_2(OH_2\text{-}\kappa O)](OSO_2CF_3)_3\cdot(H_2O)(C_4H_{10}O)_{0.5}$. Unusual Influence of the PH and Interaction of Phosphate with Catalyst on the Reaction Rate. *J. Mol. Catal. A: Chem.* **2010**, *326* (1−2), 15−20.

(6) Serrano-Ruiz, M.; Lorenzo-Luis, P.; Romerosa, A.; Mena-Cruz, A. Catalytic Isomerization of Allylic Alcohols in Water by $[RuClCp(PTA)_2]$, $[RuClCp(HPTA)_2]Cl_2\cdot 2H_2O$, $[RuCp(DMSO\text{-}\kappa S)(PTA)_2]Cl$, $[RuCp(DMSO\text{-}\kappa S)(PTA)_2](OSO_2CF_3)$ and $[RuCp(DMSO\text{-}\kappa S)(HPTA)_2]Cl_3\cdot 2H_2O$. *Dalt. Trans.* **2013**, *42* (21), 7622.

(7) Mena-Cruz, A.; Serrano-Ruiz, M.; Lorenzo-Luis, P.; Romerosa, A.; Kathó, Á.; Joó, F.; Aguilera-Sáez, L. M. Evaluation of Catalytic Activity of $[RuClCp(dmoPTA)(PPh_3)](OSO_2CF_3)$ in the Isomerization of Allylic Alcohols in Water (DmoPTA = 3,7-Dimethyl-1,3,7-Triaza-5-Phosphabicyclo[3.3.1]Nonane). *J. Mol. Catal. A: Chem.* **2016**, *411*, 27−33.

(8) Scalambra, F.; López-Sanchez, B.; Romerosa, A. Good Isomerization of 2-Cyclohexenol by Two Ru(II) Complexes, Synthesis and Characterization of a Reaction Intermediate. *Dalt. Trans.* **2018**, *47* (46), 16398−16402.

(9) Scalambra, F.; Serrano-Ruiz, M.; Romerosa, A. Water and Catalytic Isomerization of Linear Allylic Alcohols by $[RuCp(H_2O\text{-}\kappa O)(PTA)_2]^+$ (PTA = 1,3,5-Triaza-7-Phosphaadamantane). *Dalt. Trans.* **2017**, *46* (18), 5864−5871.

(10) Batuecas, M.; Esteruelas, M. A.; García-Yebra, C.; Oñate, E. Redox Isomerization of Allylic Alcohols Catalyzed by Osmium and Ruthenium Complexes Containing a Cyclopentadienyl Ligand with a Pendant Amine or Phosphoramidite Group: X-Ray Structure of an η^3-1-Hydroxyallyl-Metal-Hydride Intermediate. *Organometallics* **2010**, *29* (9), 2166−2175.

(11) Lorenzo-Luis, P.; Romerosa, A.; Serrano-Ruiz, M. Catalytic Isomerization of Allylic Alcohols in Water. *ACS Catal.* **2012**, *2*, 1079−1086.

(12) Scalambra, F.; Lorenzo-Luis, P.; de los Rios, I.; Romerosa, A. Isomerization of Allylic Alcohols in Water Catalyzed by Transition Metal Complexes. *Coord. Chem. Rev.* **2019**, *393*, 118−148.

(13) Bellarosa, L.; Díez, J.; Gimeno, J.; Lledós, A.; Suárez, F. J.; Ujaque, G.; Vicent, C. Highly Efficient Redox Isomerisation of Allylic Alcohols Catalysed by Pyrazole-Based Ruthenium(IV) Complexes in Water: Mechanisms of Bifunctional Catalysis in Water. *Chem. - Eur. J.* **2012**, *18* (25), 7749−7765.

(14) Cadierno, V.; García-Garrido, S. E.; Gimeno, J.; Varela-Álvarez, A.; Sordo, J. A. Bis(Allyl)-Ruthenium(IV) Complexes as Highly

Efficient Catalysts for the Redox Isomerization of Allylic Alcohols into Carbonyl Compounds in Organic and Aqueous Media: Scope, Limitations, and Theoretical Analysis of the Mechanism. *J. Am. Chem. Soc.* **2006**, *128* (4), 1360−1370.
(15) Díez, J.; Gimeno, J.; Lledós, A.; Suárez, F. J.; Vicent, C. Imidazole Based Ruthenium(IV) Complexes as Highly Efficient Bifunctional Catalysts for the Redox Isomerization of Allylic Alcohols in Aqueous Medium: Water as Cooperating Ligand. *ACS Catal.* **2012**, *2* (10), 2087−2099.
(16) Serrano-Ruiz, M.; Imberti, S.; Bernasconi, L.; Jadagayeva, N.; Scalambra, F.; Romerosa, A. Study of the Interaction of Water with the Aqua-Soluble Dimeric Complex $[RuCp(PTA)_2$-μ-CN-1κC:2κ^2N-$RuCp(PTA)_2](CF_3SO_3)$ (PTA = 1,3,5-Triaza-7-Phosphaadamantane) by Neutron and X-Ray Diffraction in Solution. *Chem. Commun.* **2014**, *50* (78), 11587−11590.
(17) Soper, A. K. *Empirical Potential Structure Refinement - EPSRshell: A User's Guide*; RAL Tech. Rep. RAL-TR-2011-012; STFC, 2011.
(18) Scalambra, F.; Holzmann, N.; Bernasconi, L.; Imberti, S.; Romerosa, A. Water Participation in Catalysis: An Atomistic Approach to Solvent Effects in the Catalytic Isomerization of Allylic Alcohols. *ACS Catal.* **2018**, *8* (5), 3812−3819.
(19) The Cambridge Crystallographic Data Centre (CCDC). https://www.ccdc.cam.ac.uk/ (accessed June 6, 2020).
(20) Romerosa, A.; Scalambra, F. Non-Covalent Interactions of Water with Metal Complexes in Solution. *In Non-covalent Interactions in the Synthesis and Design of New Compounds* **2016**, 83−99.
(21) Han, X.; Lee, R.; Chen, T.; Luo, J.; Lu, Y.; Huang, K. W. Kinetic Evidence of an Apparent Negative Activation Enthalpy in an Organocatalytic Process. *Sci. Rep.* **2013**, *3* (1), 2557.
(22) Scalambra, F.; Holzmann, N.; Bernasconi, L.; Imberti, S.; Romerosa, A. The Interaction of Water with Cis and Trans $\{Ru(Bpy)_2(PTA)_2\}^{2+}$ (PTA = 1,3,5-Triaza-7-Phosphaadamantane) Studied by Neutron Scattering and Ab Initio Calculations. *Eur. J. Inorg. Chem.* **2019**, *2019* (8), 1162−1169.
(23) Elschenbroich, C. *Organometallics*, 3rd ed.; Wiley-VCH, 2006; p 206.
(24) Caramori, G. F.; Garcia, L. C.; Andrada, D. M.; Frenking, G. Ruthenophanes: Evaluating Cationπ Interactions in $[Ru(\eta^6$-$C_{16}H_{12}R_4)(NH_3)_3]^{2+/3+}$ Complexes. A Computational Insight. *Organometallics* **2014**, *33* (9), 2301−2312.
(25) Holzmann, N.; Stasch, A.; Jones, C.; Frenking, G. Comparative Study of Phosphine and N-Heterocyclic Carbene Stabilized Group 13 Adducts $[L(EH_3)]$ and $[L_2(E_2H_N)]$. *Chem. - Eur. J.* **2013**, *19* (20), 6467−6479.

https://dx.doi.org/10.1021/acs.organomet.0c00585
Organometallics 2020, 39, 4491−4499